BigBrain: Automated Cortical Parcellation and Comparison with Existing Brain Atlases

Marc Fournier(✉), Lindsay B. Lewis, and Alan C. Evans

Brain Imaging Centre, Montreal Neurological Institute,
McGill University, Montreal, Canada
{marc.fournier2,lindsay.lewis,alan.evans}@mcgill.ca

Abstract. Most available 3D human brain atlases provide information only at a macroscopic level, while 2D atlases are often at a microscopic level but lack 3D integration. A 3D atlas defined upon fine-grain anatomical detail of cortical layers and cells is necessary to fully understand neurobiological processes. "BigBrain," a high-resolution 3D model of a human brain at nearly cellular resolution, was released in 2013. This unique dataset enables the extraction of microscopic data for utilization in brain mapping, modeling and simulation. We propose an automated 3D cortical parcellation of the BigBrain volume into functionally-meaningful areas in order to create a modern high-resolution 3D cytoarchitectural atlas that will complement existing brain atlases. We use a distance metrics-based framework for BigBrain parcellation, and perform comparative analyses of our results with existing atlases (Brodmann and JuBrain atlases). This work has immediate application in teaching, neurosurgery, cognitive neuroscience, and imaging-based brain mapping.

Keywords: Brain atlases · Cortical cytoarchitecture · Segmentation and parcellation · Brain mapping · Image registration · Computational neuroscience

1 Introduction

Reference brains in human brain mapping are indispensable tools, enabling integration of multimodal data into a common framework. However, most presently available human brain atlases do not provide information beyond the macroscopic level. Fine-grain anatomical resolution of cortical layers, columns, microcircuits, and cells is necessary to fully understand neurobiological processes.

In 2013 "BigBrain" [1], a high-resolution digital 3D model of a human brain reconstructed from 7,404 histological sections at a nearly cellular isotropic resolution of 20 μm, was created. The dataset is publicly available and includes 3D tissue classification as well as cortical surface extraction.

In this paper, we propose a 3D automated cortical parcellation of the BigBrain volume into functionally-meaningful areas, which should complement existing brain atlases such as the Brodmann atlas [2] and JuBrain atlas [3]. Although the 3D Brodmann atlas is widely used in neuroimaging, it is not a gold standard, neither validated

H. Müller et al. (Eds.): MCV/BAMBI 2016, LNCS 10081, pp. 14–25, 2017.
DOI: 10.1007/978-3-319-61188-4_2

nor based on robust cytoarchitectural boundaries. The JuBrain atlas is, like our current work, a high resolution cytoarchitectural atlas; however it consists of an initial 2D partial manual segmentation prior to its reconstruction in 3D. The 2D manual segmentation is guided by algorithms which utilize a local gray level index [4]. Due to the intensive manual nature of this segmentation, there are many areas of the JuBrain atlas that are not yet complete.

Previous work on 3D automated methods to parcellate brain images has been done using different imaging modalities of standard resolution such as MRI [5], fMRI [6], DTI [7] and SPECT [8]. These methods have been designed to operate at the macroscopic scale and most of them [5, 7, 8] propose parcellation schemes based on Mahalanobis and Euclidean distance metrics. While our parcellation framework is designed to operate on cytoarchitecture at the microscopic scale, it is similarly based on distance metrics including Mahalanobis and Euclidean distances.

Although parcellation of brain cytoarchitectural histology data has been addressed previously, in most cases the parcellation is done on 2D sections, and only afterwards are the segmented structures reconstructed in 3D [9, 10]. This approach restricts the definition of cytoarchitectural boundaries to two dimensions, on a single section at a time. Our new method overcomes this restriction and allows the detection of boundaries in 3D. Moreover, in contrast to previous work where cytoarchitectural boundaries are typically manually delineated by experts, our proposed method is automated.

It should be noted that recent work has also been done on the manual segmentation of the BigBrain volume in specific areas such as substructures of basal ganglia [11], with immediate clinical applications in neurosurgery [12]. The new cytoarchitectural brain atlas that we are currently proposing (again, which is automated and extends across the entire cortex) will be additionally useful for many applications in clinical and fundamental brain research, in all areas where the ubiquitous 3D Brodmann atlas is used.

The nature of the BigBrain dataset is unique. On the one hand, previous automated parcellation methods proposed for macroscopic MR images were not designed to assess cytoarchitectural boundaries. On the other hand, manual and semi-automated methods proposed to parcellate 2D cellular-level cytoarchitectural sections are not suited for the 3D volume of the BigBrain at near-cellular resolution. Therefore, the parcellation method described in this paper is especially designed for the BigBrain and inspired from previous work in both fields.

Derived from the BigBrain dataset, the goal of the proposed atlas is therefore twofold; (1) to provide a much more modern, high level of resolution, and (2) to be defined upon cytoarchitectural boundaries truly detected in 3D. In order to compare our parcellation of the BigBrain to other existing atlases, we used the method described in [13], which proposes a comprehensive set of measures for quantitative comparison of anatomical parcellations of brain atlases. This method allows the evaluation of atlases with differing numbers of regions. It is an interesting feature for the analysis of our results that the generated parcellations are likely to have different numbers of final regions. To perform our analysis, we selected a subset of the measures proposed in that method.

2 Materials and Methods

2.1 Material: BigBrain Volume, Brodmann and JuBrain Atlases

The BigBrain volume is available in various file formats and reference spaces (https://bigbrain.loris.ca). In this work, in order to avoid any distortion that may be introduced by additional processes such as registration into stereotaxic space, we used the 2015 version of the BigBrain 3D reconstructed volume in its native histological space. Such distortion could otherwise have a negative impact on parcellation results. To define the cortical mantle, which consists of voxels labeled as gray matter, we used the available 3D classified volume image and gray and white matter surfaces, extracted at 200 μm.

Additionally, we used the 3D Brodmann atlas provided with MRIcron software (available at http://www.mccauslandcenter.sc.edu/mricro/mricron). The atlas was registered to the BigBrain volume in order to compare our parcellations of the BigBrain to the projected Brodmann areas. We focused our work on the left hemisphere of the brain since the Brodmann atlas was initially defined on the left hemisphere. The right hemisphere of the atlas is a symmetric copy of the left.

For specific regions such as visual cortex, we also chose to compare our parcellation results with the JuBrain atlas (available at http://www.fz-juelich.de/inm/inm-1/EN/Forschung/JuBrain/Jubrain_Webtools/Jubrain_Webtools_node.html). The ongoing construction of this atlas is performed using a semi-automated parcellation method [4] previously introduced to assist experts in delineation of cytoarchitectural boundaries upon 2D slices. This method uses distance metrics to capture differences between cytoarchitectural profiles.

We adapted this method for the BigBrain dataset, but because this method was designed to operate at a cellular resolution of 1 μm, we failed to obtain significant parcellations. Image processing tools provided by this method count individual cell bodies in a region of interest. At the resolution of the BigBrain (20 μm), individual cells are not visible; therefore this method was not appropriate to achieve our goal.

2.2 Methods: Multilevel Parcellations Algorithm Approach (Overview)

Our analysis consisted of an initialization phase followed by a tri-level parcellation approach (Fig. 1). At the initialization phase, described in Sect. 2.3 below, initial profiles (163,842 3D bars) were defined and dropped across the cortical mantle, maximizing coverage while avoiding overlap. Using a Scale-Invariant Feature Transform (SIFT) algorithm these initial profiles were triaged down to 1,071 starting profiles that represented the maximally homogenous centers within groups of profiles exhibiting similar information (while being maximally distant from borders of profiles exhibiting different information). The tri-level parcellation approach is based on a distance metric framework, which is described in Sect. 2.4 below.

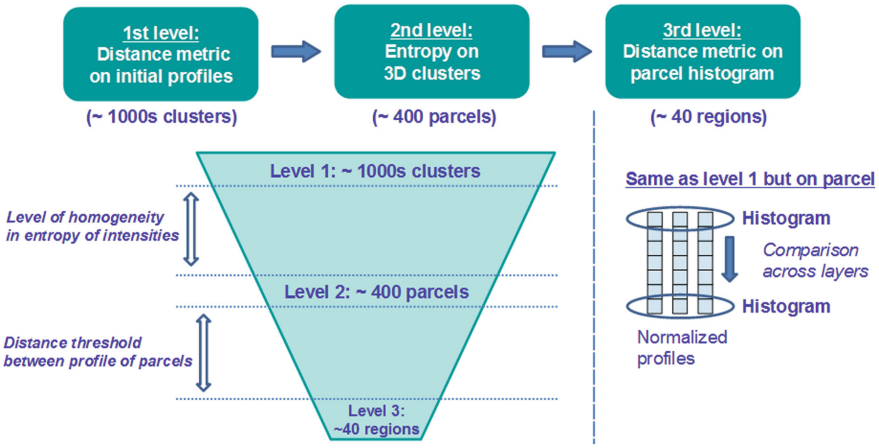

Fig. 1. Multilevel parcellation algorithm divided into three levels from fine to coarse.

At the first level of parcellation, described in Sect. 2.5 below, distances between the starting profiles and their neighbors were computed. Similar neighboring profiles were collapsed together to form 3D clusters in a data-driven, region-growing process which yielded 1,071 clusters. The second (intermediate) level of parcellation, described in Sect. 2.6 below, was introduced in order to bridge the gap between the first and third levels of parcellation. The entropy of the previously obtained 3D clusters was used to merge similar ones, reducing these 1,071 clusters to $\sim$400 parcels (entropy thresholds were user-defined and adjusted to target a number that is one order of magnitude higher than the final target in the third level). At the third level of parcellation, described in Sect. 2.7 below, distance metrics were again employed, this time onto the histograms of the previously obtained $\sim$400 parcels in order to reduce them to $\sim$40 final regions (distance metric thresholds were also user-defined and adjusted to target a comparable number of regions as the Brodmann atlas).

2.3 Methods: Initial Profiles and Algorithm Starting Points (Initialization)

First, initial profiles were created over the entire cortical mantle of the BigBrain. A profile is a column which begins with a voxel on the gray matter surface, transversing down through the cortical layers in the direction of the gray matter surface normal vector, and ends with a voxel on the white matter surface, as schematized in Fig. 2. By applying the Laplace equation as proposed in [14], we determined that using a 3D 18-connected neighborhood for voxels along the path would provide maximum density of profiles without overlap. Next, in order to assure robustness of profiles to effects of curvature on layer compression, we used an equivolumic cortical depth model [15]. Finally, all profiles were normalized to straight vectors of identical length, with values corresponding to voxel intensities across cortical layers.

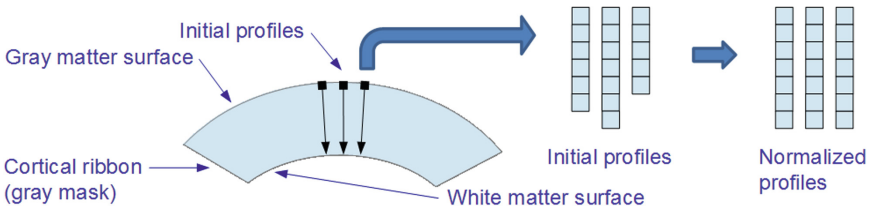

Fig. 2. Initial profiles creation: 3D bars across cortical layers of the BigBrain volume.

The process outlined above yielded a total of 163,842 initial profiles. Next, it was necessary to reduce this number to a biologically representative set of key points (1,071) to be used as input to the parcellation algorithm.

To choose this set of key points, first, we used the SIFT (Scale-Invariant Feature Transform) algorithm [16], which identifies features of interest in a 2D image, and adapted it to determine 3D key points of interest. We used Eq. (1) to compute in 3D the gradient amplitude and angles of each voxel.

$$Amp = \sqrt{G_x^2 + G_y^2 + G_z^2}; \theta = a\tan\left(\frac{G_y}{G_x}\right); \varphi = a\tan\left(\frac{G_z}{\sqrt{G_x^2 + G_y^2}}\right) \quad (1)$$

Then we constructed an orientation histogram as proposed in [17] for the 3D neighborhood around a given interest point by dividing θ and ϕ into bins of equal size. While working in 3D, it was also necessary to normalize the values added to each bin by the area of the bin as described in [18]. This corresponds to the solid angle Ω computed using Eq. (2). The values added to the histogram were computed using Eq. (3) where (x_n, y_n, z_n) represented the location of the voxel being added to the histogram of the interest point.

$$\Omega = \int_{\varphi}^{\varphi + \Delta\varphi} \int_{\theta}^{\theta + \Delta\theta} \sin\theta \, d\theta \, d\varphi = \Delta\varphi[\cos\theta - \cos(\theta + \Delta\theta)] \quad (2)$$

$$hist = \frac{1}{\Omega} Amp(x_n, y_n, z_n) e^{-\left[\frac{(x-x_n)^2 + (y-y_n)^2 + (z-z_n)^2}{2\sigma^2}\right]} \quad (3)$$

In this manner, we were able to obtain preliminary key points that were more likely to be close to the parcels' borders (where information was most heterogeneous).

Second, we performed an additional step to shift those key points away from each border and instead more centrally, toward profiles exhibiting maximally homogeneous information. Accordingly, our starting points would be in the presumed center of a given region. To accomplish this, we tessellated the key points by generating a tetrahedral mesh based on a 3D Delaunay triangulation algorithm [19]. Then, we computed its dual mesh (also known as the Voronoi diagram). The set of voxels located in the center of the tetrahedrons (corresponding to the Voronoi diagram vertices) were used as the starting points of our parcellation algorithm.

2.4 Methods: Distance Metrics Definitions (Used at First and Third Levels)

Our parcellation algorithm is based upon measurements of distance metrics, assessed between initial profiles (first level) and then again between 3D parcels (third level). Distance metrics serve as similarity criteria, comparing the (dis)similarity of intensity properties. In this analysis, we tested a subset of the distance metrics surveyed in [20] in order to identify the most suitable metric for our parcellation task. Our goal was to select those metrics that were most informative about different, complementary features, while disregarding those that were redundantly informative about similar features. The distance metrics tested are listed in Table 1.

Table 1. List of distance metrics used in the parcellation algorithm

City block	$d(x,y) = \sum_{i=1}^{n} \lvert x_i - y_i \rvert$	Canberra	$d(x,y) = \sum_{i=1}^{n} \frac{\lvert x_i - y_i \rvert}{\lvert x_i + y_i \rvert}$
Euclidean	$d(x,y) = \sqrt{\sum_{i=1}^{n} (x_i - y_i)^2}$	Squared chord	$d(x,y) = \sum_{i=1}^{n} \left(\sqrt{x_i} - \sqrt{y_i}\right)^2$
Minkowski	$d(x,y) = \left(\sum_{i=1}^{n} \lvert x_i - y_i \rvert^p\right)^{1/p}$	Squared Chi	$d(x,y) = \sqrt{\sum_{i=1}^{n} \frac{(x_i - y_i)^2}{\lvert x_i + y_i \rvert}}$

In the first column of Table 1, we selected widely used distances of the same L_p family, with City block and Euclidean distances being particular cases of the Minkowski distance when $p = 1$ and $p = 2$, respectively. For Minkowski distance, we selected $p = 3$ in order to obtain better results. In the second column of Table 1, we selected other distances among the most used in their respective families: Canberra distance belongs to L_1 family, Squared chord to *Fidelity* family, and Squared Chi to *Squared* L_2 family. In addition to the six Table 1 distance metrics that we obtained from [20], we additionally tested the Mahalanobis distance [21], defined by Eq. (4).

$$d(x,y) = \sqrt{(x-y)^T S^{-1} (x-y)} \; where: \; S = covariance\ matrix \tag{4}$$

It is worth noting that if the elements of x and y are independents, then the covariance matrix will be the identity one, and in that case the Mahalanobis distance would be equal to the Euclidean distance. In two dimensions, equal distances from a center point are represented by circles for the Euclidean distance, and for the Mahalanobis distance they are represented by ellipses.

2.5 Methods: Distance Metrics (First Level)

For each of the seven distance metrics selected, the following procedure (schematized in Fig. 1) was independently performed. As already described, the initialization phase considered all initial profiles (163,842), using the adapted 3D SIFT algorithm in order to select the starting profiles (1,071).

Next, distances between starting profiles and their neighbors were computed. Neighboring profiles with distances under a predefined threshold were labeled and collapsed together to form 3D clusters. In a region-growing process, the scope moved from starting profiles to the labeled neighbor ones. Distances were then computed between labeled profiles and their nearest neighbors. This process terminated when all of the initial profiles had ultimately been assigned to an existing cluster. The distance threshold was initially set at a low value. If initial profiles remained unlabeled, the process iterated with an increased threshold until all profiles belonged to a cluster.

Of additional interest, this highly detailed parcellation (1,071 clusters) may be advantageously combined with recently emerging new atlases at high-resolution such as [22], which defines ~900 neuroanatomically precise subdivisions based on genomic transcriptome distributions of the brain.

2.6 Methods: Entropy Measurements (Second Level)

In the second level of parcellation, using entropy measurements, the 1,071 3D clusters were input as seeds to grow ~400 parcels. This intermediate level of parcellation was introduced in order to bridge the gap between the first and third level. In practice, this is useful to target a specific number of final regions with unit increment. Our entropy measurement [23] was defined by Eq. (5).

$$E(p(x)) = \sum\nolimits_{x \in X} p(x) \log(p(x)) \; where : \; p(x) = histogram \; of \; x \tag{5}$$

By definition this measure is not a metric because it does not satisfy some of the metric conditions such as symmetry and triangle inequality. Entropy is a statistical measure used to characterize the texture of our clusters obtained after the first level of parcellation. It gives a quantitative appreciation of homogeneity of a cluster in terms of intensities of its voxels. In order to compute the entropy measurement, we used 256 bins to construct the histogram counts of the clusters.

If two neighboring clusters exhibited similar entropy, they were regrouped together as a parcel, and the algorithm continued moving outward. If not, the algorithm stopped and it was defined as an edge or boundary of the parcel. The level of similarity required to merge clusters was set in such a way to obtain a number of parcels which is an order of magnitude higher than the number of final regions targeted. As shown in Fig. 1, since we were ultimately targeting close to 40 final regions for comparison with Brodmann areas (41 in the atlas used), the intermediate number was set to ~400 parcels.

2.7 Methods: Distance Metrics (Third Level)

At the third level of parcellation, histograms were constructed to characterize the distribution of the intensities of voxels across cortical layers in all previously obtained parcels (~400). Then, the same distance metric (used on single voxels of initial profiles at first level, described above in Sect. 2.5) was used in a similar way on the histograms of parcels. Here, the distance threshold between neighbor parcels was set to obtain the targeted number of final regions (~40).

3 Results

The proposed parcellation pipeline was processed with each metric. Results were selected based upon global similarity of parcellations in comparison to the Brodmann atlas, using a similarity index value yielded by a region-level concordance analysis proposed in [13]. The obtained results do not necessarily have exactly 41 regions; rather, the similarity index was used to target the best matches compared to Brodmann areas. The Mahalanobis distance metric obtained the highest similarity index score, and was therefore identified as the metric to best map the Brodmann parcellation scheme onto the BigBrain volume. Accordingly, its similarity index was used to normalize the similarity index of all other metrics in order to compare their results. Figure 3 shows the normalized indices and the number of regions for each metric result.

Distance Metrics	Normalized Similarity	Number of Regions
Mahalanobis	1,00	37
Squared chord	0,96	42
Canberra	0,81	41
City block	0,79	41
Squared Chi	0,76	38
Euclidean	0,70	36
Minkowski	0,66	38

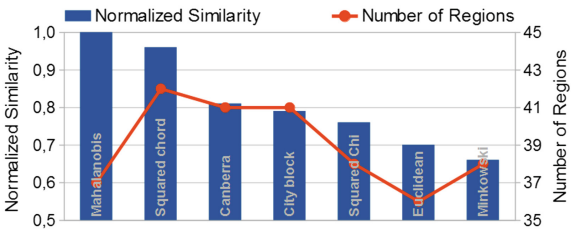

Fig. 3. Evaluation of the distance metrics tested based on their similarity indices.

In Fig. 3, the metrics are ranked in decreasing order of similarity index. The second one in line is the Squared chord metric, which is very close to the Mahalanobis metric, and thus does not provide substantially different information. Both have different numbers of regions which do not exactly correspond to the number of Brodmann areas. The average number of regions for all metrics is 39, which is two regions less than the Brodmann atlas. The Canberra and City block metrics have 41 regions (same as the Brodmann atlas) and both have very similar indices, ranked third and fourth.

Figure 4 shows the parcellation result of the Mahalanobis metric, which was found to be the most similar to the Brodmann atlas based on the previous analysis. Figure 4(a) shows the Brodmann areas registered to the BigBrain left hemisphere, while Fig. 4(b) shows the Mahalanobis parcellation result. Both color codes are similar but they do not exactly match since the number of regions/areas are not the same. Figure 4(c) shows a quantitative analysis of volume concordance between Brodmann areas and our parcellation results. Mutual overlapping volume distribution is quantified between our result and the Brodmann atlas.

In Fig. 4(c), the blue columns show the fraction of the volume of a Brodmann area which is overlapped by the BigBrain parcellation region covering most of that area's volume. Likewise, the orange columns show the fraction of the volume of the BigBrain parcellation region (previously identified) which is overlapped by that same Brodmann

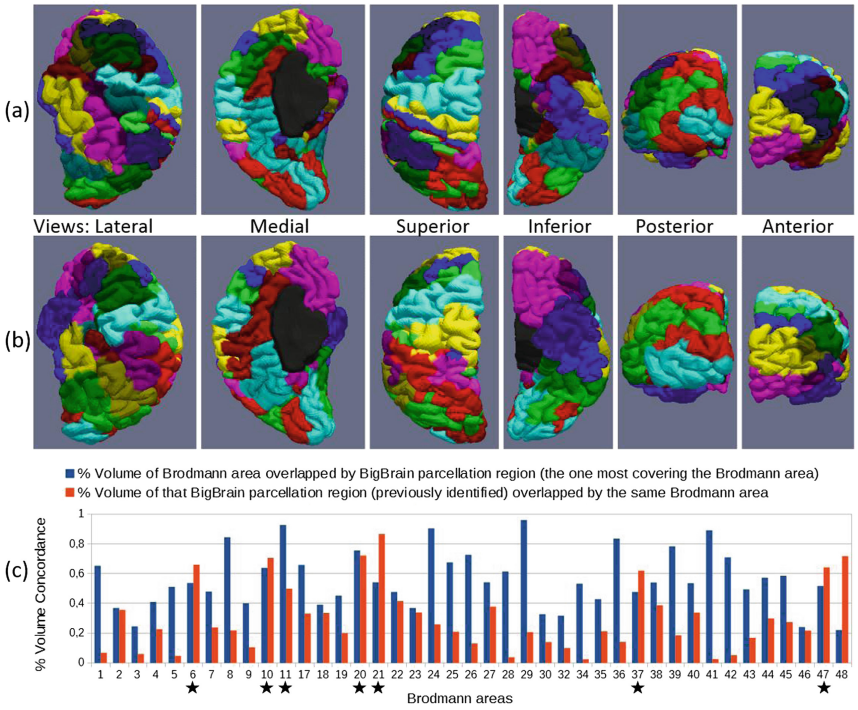

Fig. 4. Comparison of BigBrain parcellation with Brodmann atlas using Mahalanobis distance. (a) BigBrain left hemisphere with Brodmann areas. (b) BigBrain parcellation results using color coding similar to Brodmann areas in (a) to highlight concordance. (c) Chart of concordance between Brodmann areas and BigBrain parcellation regions. (Color figure online)

area. If a perfect match were to be attained for a specific Brodmann area, the value of both blue and orange columns for that area would be 1. The stars below selected Brodmann areas denote areas with high concordance, represented by higher values in both (blue and orange) columns.

Figure 5 shows (a) Mahalanobis and (b) Canberra results compared to JuBrain atlas in the visual cortex (Squared Chord was omitted because it demonstrated high similarity to Mahalanobis). These parcellations have been adapted by targeting a higher number of final regions in order to match the level of detail of the JuBrain segmentation in the visual cortex. In Fig. 5, the numbered arrows designate boundaries successfully detected by the parcellation algorithm compared to JuBrain areas, while lettered circles designate where the distance metrics have failed to detect some JuBrain areas.

This qualitative analysis highlights the complementarity of the distance metric results. For example, both failures with Mahalanobis (circles A and B, Fig. 5(a)) were successfully detected with Canberra (arrows 1 and 2, Fig. 5(b)) and inversely the failure with Canberra (circle A, Fig. 5(b)) was successfully detected with Mahalanobis (arrow 2, Fig. 5(a)). This observation demonstrates that, according to the JuBrain atlas, combining these two metrics may lead to a better parcellation. Ongoing work focuses on automated linear combination of metrics in order to optimize the results.

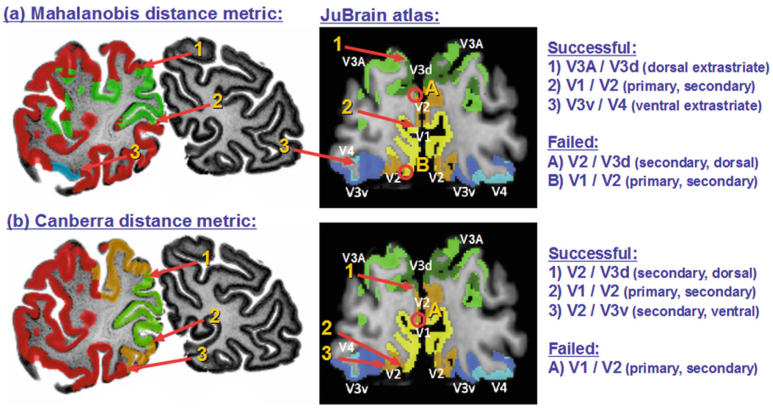

Fig. 5. Comparison of BigBrain parcellation with JuBrain atlas with focus on the visual cortex. (a) Mahalanobis distance compared to JuBrain. (b) Canberra distance compared to JuBrain.

4 Conclusion

We have proposed an automated parcellation of the BigBrain volume in order to provide a unique high-resolution modern cytoarchitectural 3D atlas. This work has immediate value across a broad range of applications, including teaching, neurosurgery, cognitive neuroscience, and imaging-based brain mapping. Our parcellation framework is based upon distance metrics, and we performed comparative analyses of our results with existing brain atlases. Future work will include refinement of the parcellation using consensus between complementary distance metrics, and validation of results from a functional neuroanatomy perspective.

Acknowledgements. We acknowledge funding support from the Canadian Institutes of Health Research (CIHR) and from Canada's Advanced Research and Innovation Network (CANARIE). We thank Compute Canada for continued support accessing the Compute Canada HPC grid through the CBRAIN software portal. We also thank Svenja Caspers for helpful discussion and providing expertise in neuroanatomy as well as Katrin Amunts and Karl Zilles from the Jülich Research Centre in Germany.

References

1. Amunts, K., Lepage, C., Borgeat, L., Mohlberg, H., Dickscheid, T., Rousseau, M.E., Bludau, S., Bazin, P.L., Lewis, L.B., Oros-Peusquens, A.M., Shah, N.J., Lippert, T., Zilles, K., Evans, A.C.: BigBrain: an ultrahigh-resolution 3D human brain model. Science **340**, 1472–1475 (2013)
2. Brodmann, K.: Vergleichende Lokalisationslehre der Grosshirnrinde. Johann Ambrosius Bart, Leipzig (1909)

3. Mohlberg, H., Eickhoff, S.B., Schleicher, A., Zilles, K., Amunts, K.: A new processing pipeline and release of cytoarchitectonic probabilistic maps – JuBrain. In: 18th Annual Meeting of the Organization for Human Brain Mapping, Beijing, China (2012)
4. Schleicher, A., Palomero-Gallagher, N., Morosan, P., Eickhoff, S.B., Kowalski, T., de Vos, K., Amunts, K., Zilles, K.: Quantitative architectural analysis: a new approach to cortical mapping. Anatomy Embryol. **210**, 373–386 (2005)
5. Hemanth, D.J., Selva Vijila, C.K., Selvakumar, A.I., Anitha, J.: Distance metric-based time-efficient fuzzy algorithm for abnormal magnetic resonance brain image segmentation. Neural Comput. Appl. **22**, 1013–1022 (2013)
6. Sanchez-Panchuelo, R.M., Besle, J., Beckett, A., Bowtell, R., Schluppeck, D., Francis, S.: Within-digit functional parcellation of brodmann areas of the human primary somatosensory cortex using functional magnetic resonance imaging at 7 tesla. J. Neurosci. **32**, 15815–15822 (2012)
7. Kong, Y., Wang, D., Shi, L., Hui, S.C.N., Chu, W.C.W.: Adaptive distance metric learning for diffusion tensor image segmentation. PLoS ONE **9**, e92069 (2014)
8. Chaves, R., Ramírez, J., Górriz, J.M., Illán, I., Segovia, F., Olivares, A.: Effective diagnosis of alzheimer's disease by means of distance metric learning and random forest. In: Ferrández, J.M., Álvarez Sánchez, J.R., Paz, F., Toledo, F.J. (eds.) IWINAC 2011. LNCS, vol. 6687, pp. 59–67. Springer, Heidelberg (2011). doi:10.1007/978-3-642-21326-7_7
9. Uylingsa, H.B.M., Sanz-Arigita, E.J., de Vos, K., Pool, C.W., Evers, P., Rajkowska, G.: 3-D cytoarchitectonic parcellation of human orbitofrontal cortex correlation with postmortem MRI. Psychiatry Res. Neuroimaging **183**, 1–20 (2010)
10. Caspers, S., Geyer, S., Schleicher, A., Mohlberg, H., Amunts, K., Zilles, K.: The human inferior parietal cortex: cytoarchitectonic parcellation and interindividual variability. NeuroImage **33**, 430–448 (2006)
11. Altinkaya, A., Lepage, C., Lewis, L.B., Toussaint, P.J., Amunts, K., Zilles, K., Evans, A.C., Sadikot, A.F.: Ultrahigh resolution 3-d volumetric atlas of the human basal ganglia. In: 21st Annual Meeting of the Organization for Human Brain Mapping, Honolulu, USA (2015)
12. Altinkaya, A., Lepage, C., Ferreira, M., Pike, G.B., Evans, A.C., Sadikot A.F.: Registration of the bigbrain basal ganglia atlas to MNI space with surgical applications. In: 21st Annual Meeting of the Organization for Human Brain Mapping, Honolulu, USA (2015)
13. Bohland, J.W., Bokil, H., Allen, C.B., Mitra, P.P.: The brain atlas concordance problem: quantitative comparison of anatomical parcellations. PLoS ONE **4**, e7200 (2009)
14. Jones, S.E., Buchbinder, B.R., Aharon, I.: Three-dimensional mapping of cortical thickness using laplace's equation. Hum. Brain Mapping **11**, 12–32 (2000)
15. Leprince, Y., Poupon, F., Delzescaux, T., Hasboun, D., Poupon, C., Riviere, D.: Combined laplacian-equivolumic model for studying cortical lamination with ultra high field MRI (7T). In: 12th IEEE International Symposium on Biomedical Imaging, pp. 580–583. IEEE Press, New York (2015)
16. Lowe, D.G.: Distinctive image features from scale-invariant keypoints. Int. J. Comput. Vis. **60**, 91–110 (2004)
17. Toews, M., Wells, W.M.: Efficient and robust model-to-image alignment using 3D scale-invariant features. Med. Image Anal. **17**, 271–282 (2013)
18. Scovanner, P., Ali, S., Shah, M.: A 3-dimensional SIFT descriptor and its application to action recognition. In: Proceedings of the 15th ACM International Conference on Multimedia, pp. 357–360. AMC Press, New York (2007)
19. Golias, N.A., Dutton, R.W.: Delaunay triangulation and 3D adaptive mesh generation. Finite Elements Anal. Des. **25**, 331–341 (1997)
20. Cha, S.H.: Comprehensive survey on distance/similarity measures between probability density functions. Int. J. Math. Models Methods Appl. Sci. **1**, 300–307 (2007)

21. Mahalanobis, P.C.: On the generalised distance in statistics. Proc. Natl. Inst. Sci. India **2**, 49–55 (1936)
22. Hawrylycz, M.J., Lein, E.S., Guillozet-Bongaarts, A.L., Shen, E.H., Ng, L., Miller, J.A., van de Lagemaat, L.N., Smith, K.A., Ebbert, A., Riley, Z.L., et al.: An anatomically comprehensive atlas of the adult human brain transcriptome. Nature **489**, 391–399 (2012)
23. Shannon, C.E.: A mathematical theory of communication. Bell Labs Tech. J. **27**, 379–423 (1948)

http://www.springer.com/978-3-319-61187-7

Medical Computer Vision and Bayesian and Graphical Models for Biomedical Imaging
MICCAI 2016 International Workshops, MCV and BAMBI, Athens, Greece, October 21, 2016, Revised Selected Papers

Müller, H.; Kelm, B.M.; Arbel, T.; Cai, W.T.; Cardoso, M.J.; Langs, G.; Menze, B.; Metaxas, D.; Montillo, A.; Wells III, W.M.; Zhang, S.; Chung, A.C.S.; Jenkinson, M.; Ribbens, A. (Eds.)

2017, XIII, 222 p. 75 illus., Softcover
ISBN: 978-3-319-61187-7